Supporting information

Enhancement of NH_3 Production in Electrochemical N_2 Reduction by the Cu-Rich Inner Surfaces of Beveled CuAu Nanoboxes

Biva Talukdar,[†,#,○] Tung-Chun Kuo,[‡] Brian T. Sneed,[‖] Lian-Ming Lyu,[§] Hung-Min Lin,[†,⊥] Yu-Chun Chuang,[¶] Mu-Jeng Cheng[*,‡] and Chun-Hong Kuo[*,†,△]

[†]*Institute of Chemistry, Academia Sinica, Taipei 11529, Taiwan*

[#]*Sustainable Chemical Science and Technology, Taiwan International Graduate Program, Academia Sinica and National Yang Ming Chiao Tung University, Taipei 11529, Taiwan*

[○]*Department of Applied Chemistry, National Yang Ming Chiao Tung University, Hsinchu 30010, Taiwan*

[‡]*Department of Chemistry, National Cheng Kung University, Tainan 70101, Taiwan*

[‖]*Cabot Microelectronics, Aurora, Illinois 60504, United States*

[§]*Department of Materials Science and Engineering, National Tsing Hua University, Hsinchu 30013, Taiwan*

[⊥]*Department of Chemistry, National Taiwan University, Taipei 10617, Taiwan*

[¶]*National Synchrotron Radiation Research Center, Hsinchu 30076, Taiwan*

[△]*Institute of Materials Science and Engineering, National Central University, Taoyuan 32001, Taiwan*

Contact information of corresponding authors

*(M.-J. C.) E-mail: mjcheng@mail.ncku.edu.tw

*(C.-H. K.) E-mail: chunhong@gate.sinica.edu.tw

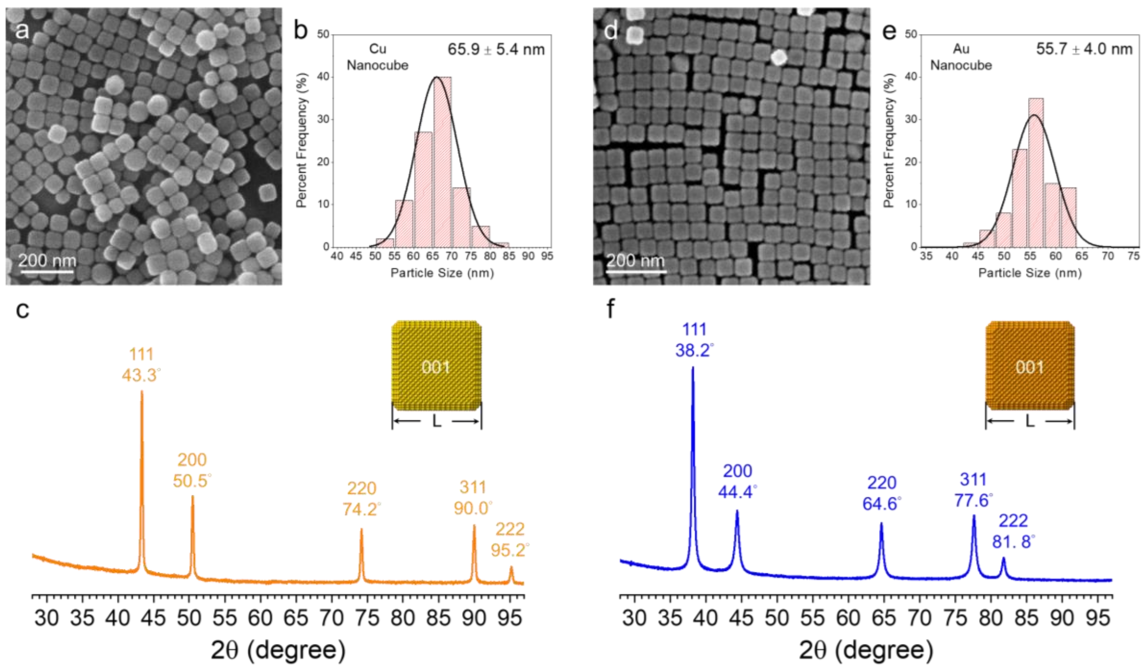

Figure S1. (a, d) SEM images, (b, e) size-distribution histograms, and (c, f) PXRD patterns of (a-c) Cu, and (d-f) Au nanocubes.

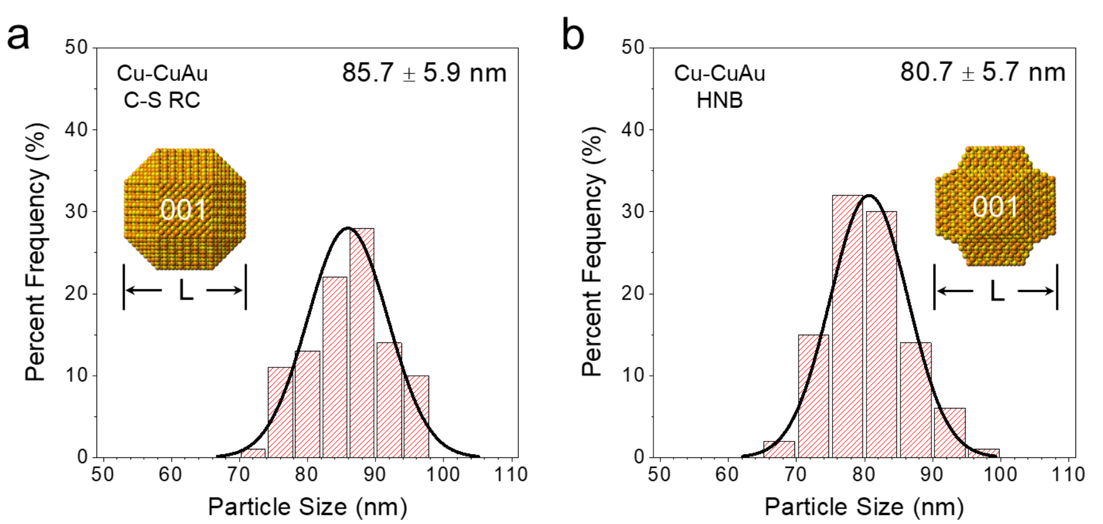

Figure S2. Size-distribution histograms of (a) rhombic cuboctahedral Cu-CuAu core-shell nanocrystals, and (b) their corresponding hollow nanocages after removing Cu cores.

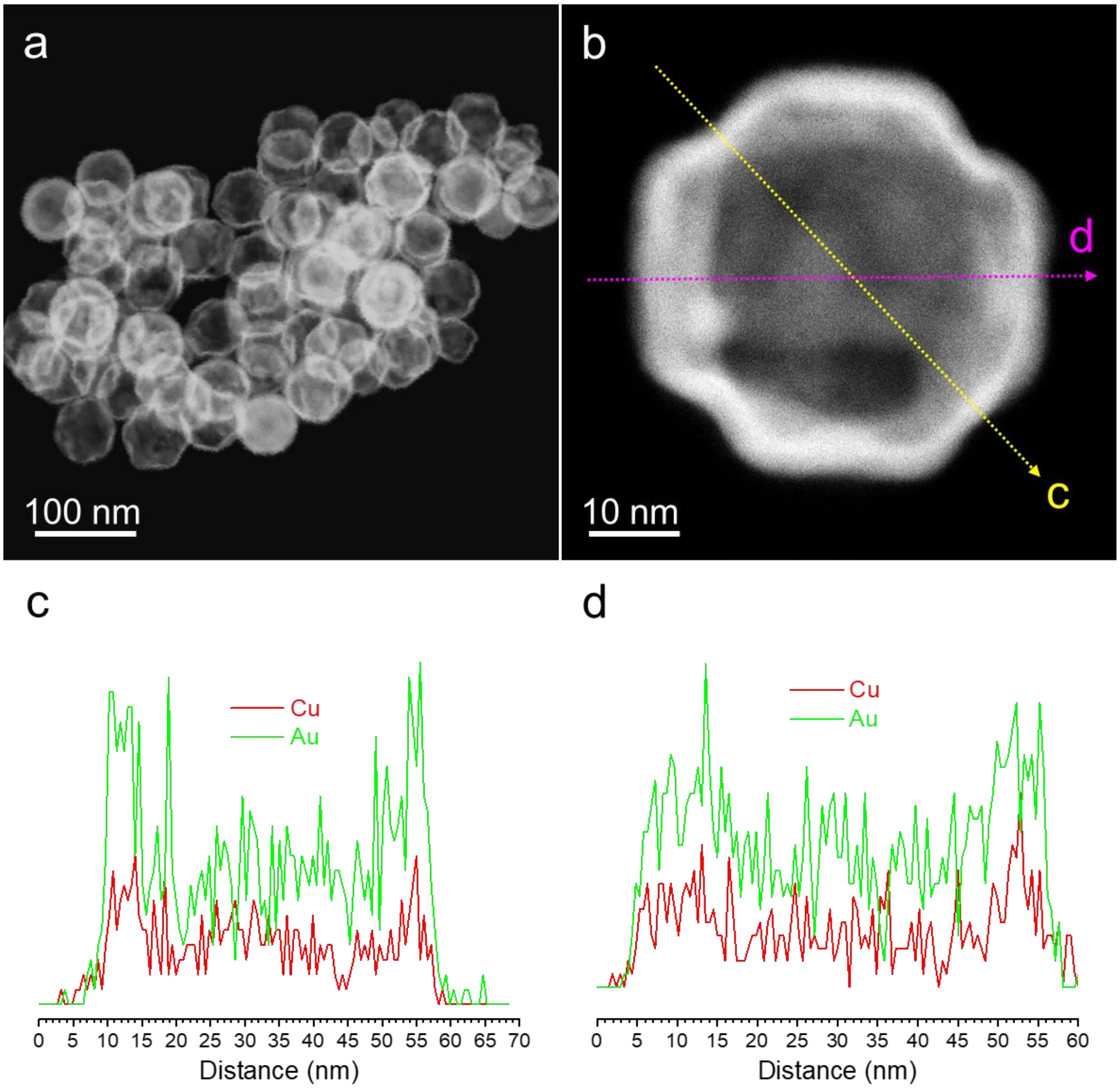

Figure S3. HAADF-STEM images of (a) multiple and (b) a single CuAu nanoboxes. The single nanocage is viewed along the [100] direction. (c, d) EDS line-scan profiles of the single nanobox along the yellow (c) and pink (d) cross sections.

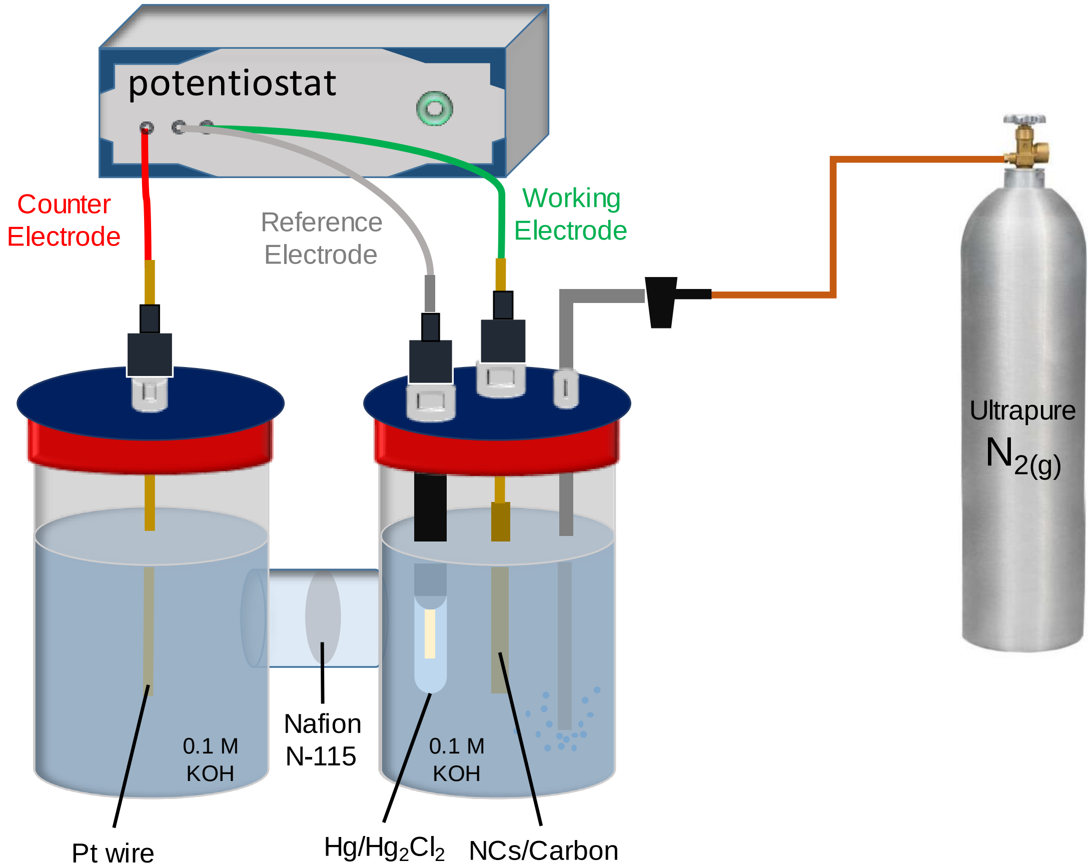

Figure S4. Schematic illustration for the setup of electrochemical N_2 reduction reaction.

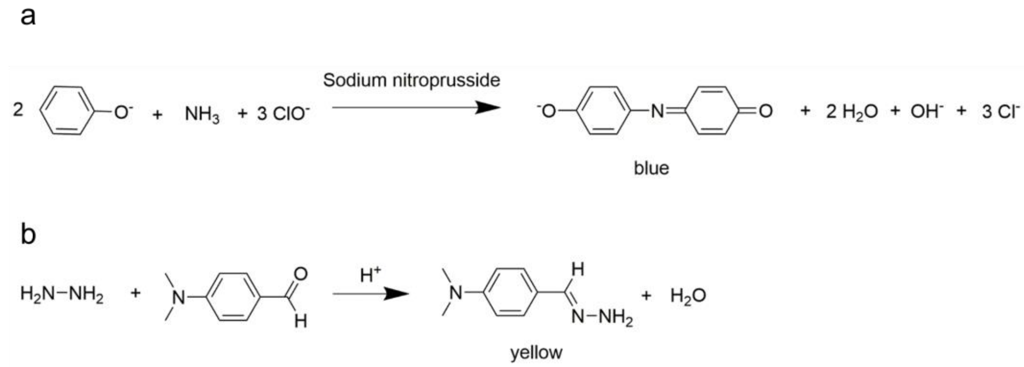

Figure S5. The condensation reactions for (a) indophenol blue method, and (b) Watt and Chrisp's Method.

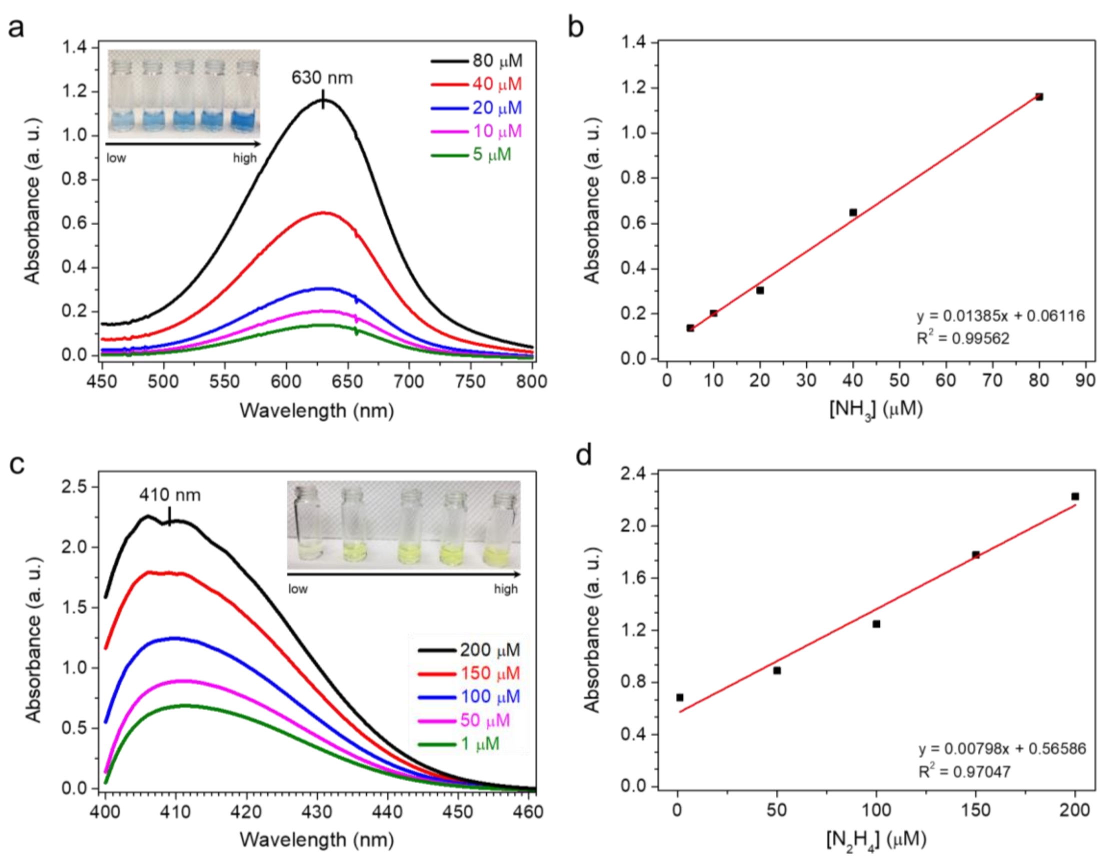

Figure S6. UV-Vis spectra and calibration plots of (a, b) indophenol blue method for NH_3 quantification and (c, d) Watt and Chrisp's method for N_2H_4 quantification.

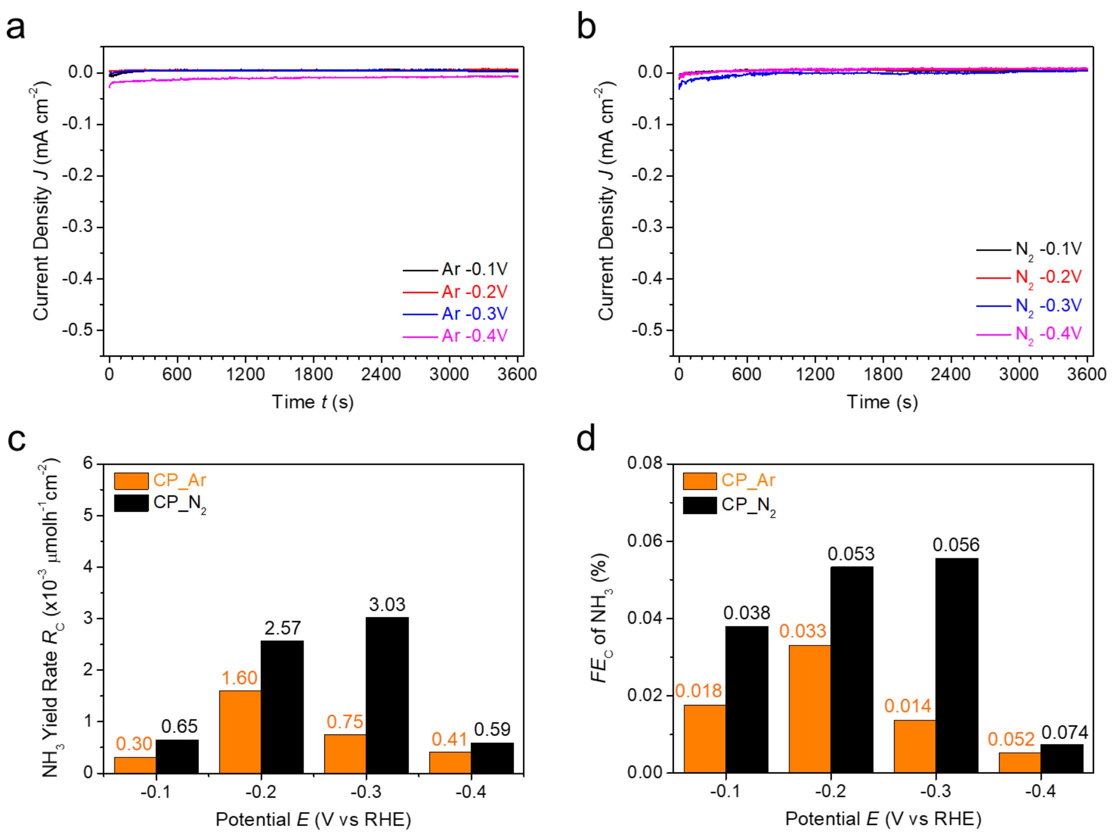

Figure S7. *J-t* plots of the bare carbon paper operated under (a) Ar and (b) N_2 flow, and their corresponding *E*-dependent distributions in (c) NH_3 yield rates and (d) Faradaic efficiencies.

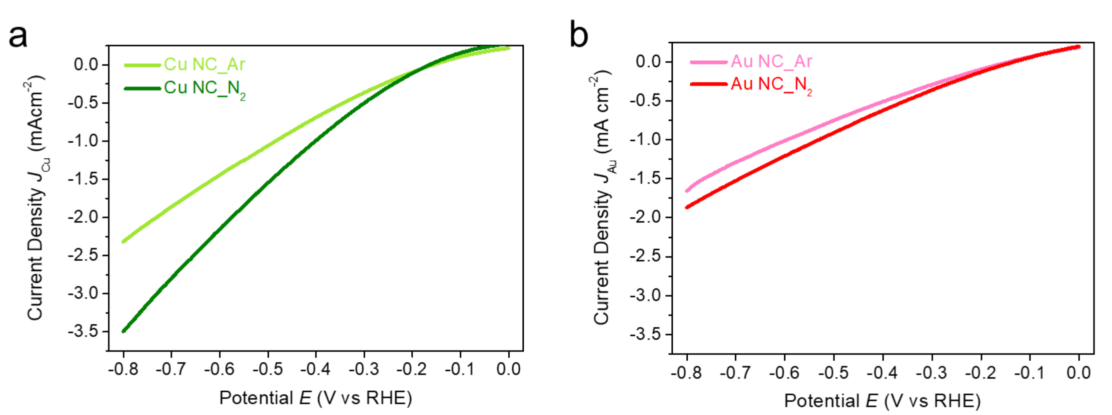

Figure S8. LSV plots of (a) Cu and (b) Au NC-catalyzed reduction under Ar and N_2 flow at the scan rate of 50 mV/s.

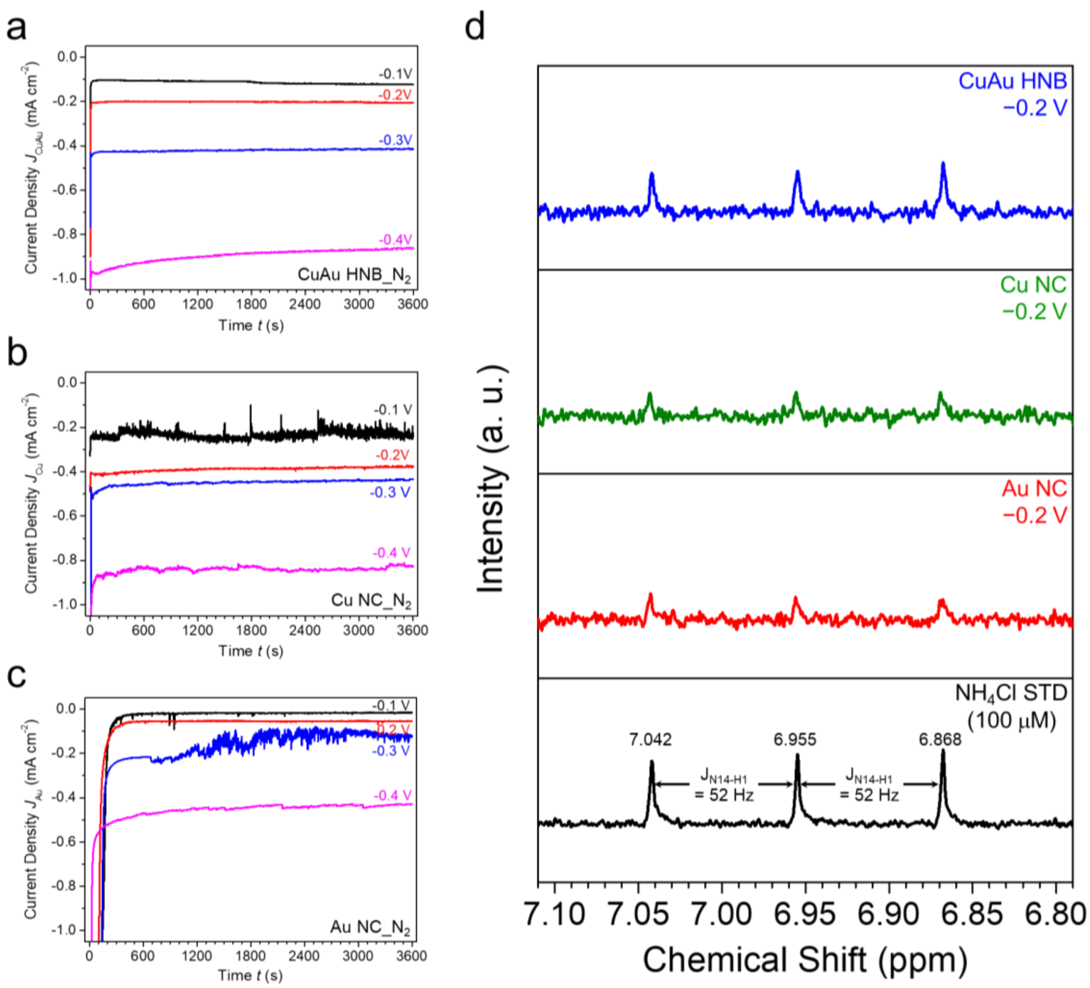

Figure S9. *J-t* plots of N_2RR catalyzed by (a) CuAu HNBs, (b) Cu NCs, and (c) Au NCs at the constant potentials of −0.1, −0.2, −0.3, and −0.4 V for an hour. (d) ^{1}H NMR spectra of the electrolyte solutions for the catalysts and a standard solution of 100 μM NH_4Cl.

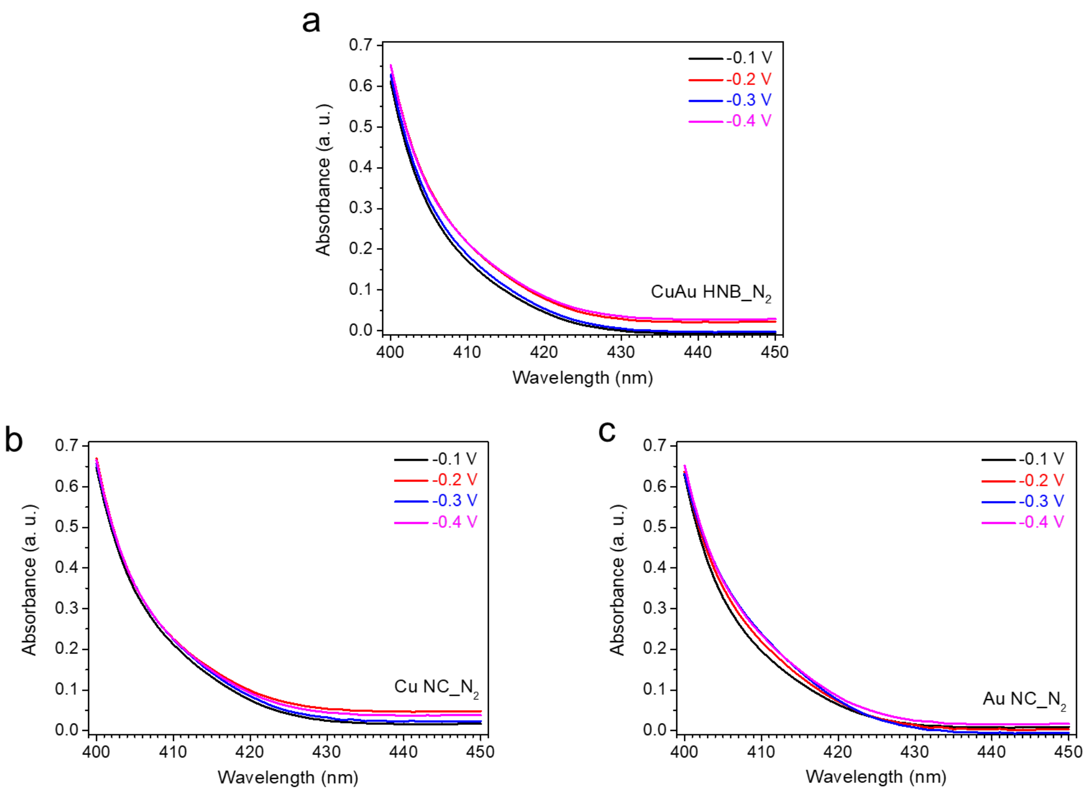

Figure S10. UV-Vis spectra measurements based on the Watt and Chrisp's method show no detectable N_2H_4 in the N_2RR catalyzed by (a) CuAu HNBs, (b) Cu NCs, and (c) Au NCs.

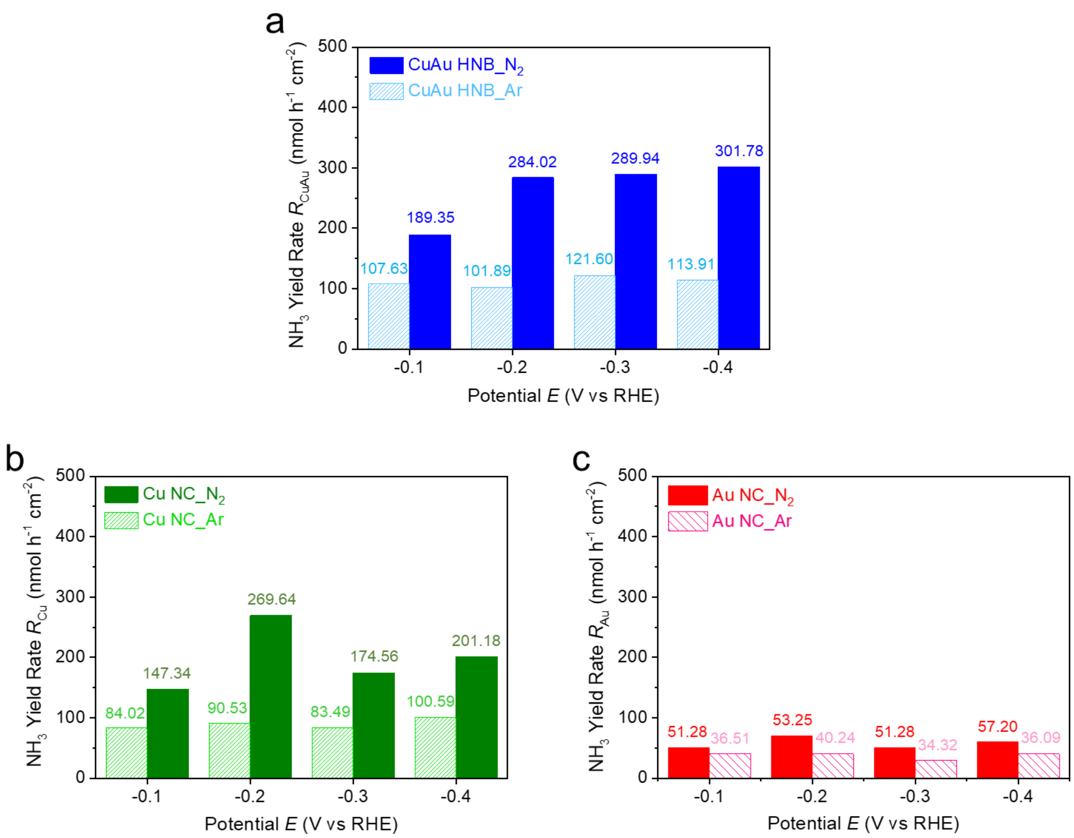

Figure S11. NH_3 yield rates of (a) CuAu HNB-, (b) Cu NC-, and (c) Au NC-catalyzed reduction reactions under Ar and N_2 flow.

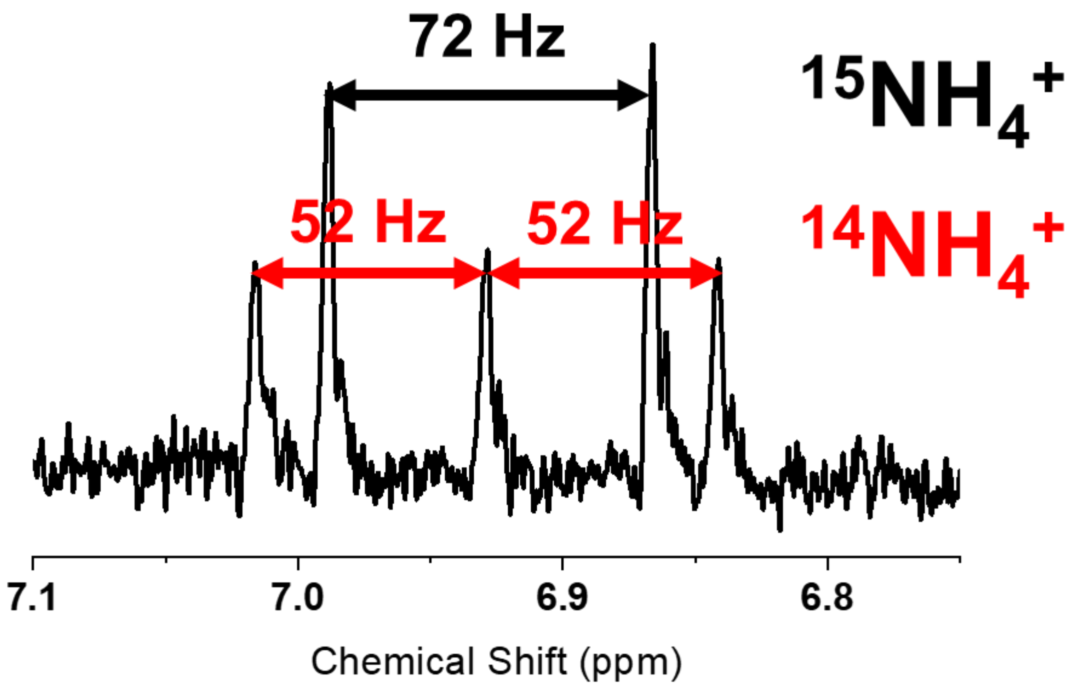

Figure S12. ^{1}H NMR spectrum of the electrolyte solution saturated with $^{15}N_2$ gas catalyzed by the HNBs. The signals of products contain the triplet peaks with a coupling constant of 52 Hz from the coupling between ^{1}H and ^{14}N (spin 1), and the doublet peaks with a coupling constant of 72 Hz due to the coupling between ^{1}H and ^{15}N (spin 1/2).

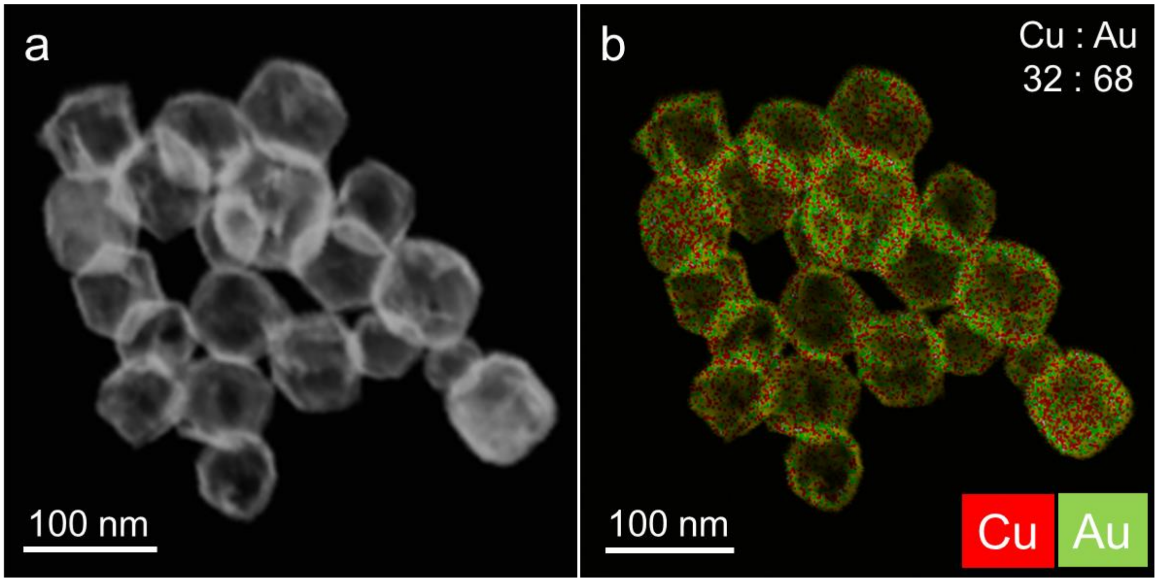

Figure S13. (a) HAADF-STEM image and (b) EDS map of CuAu HNBs after durability test.

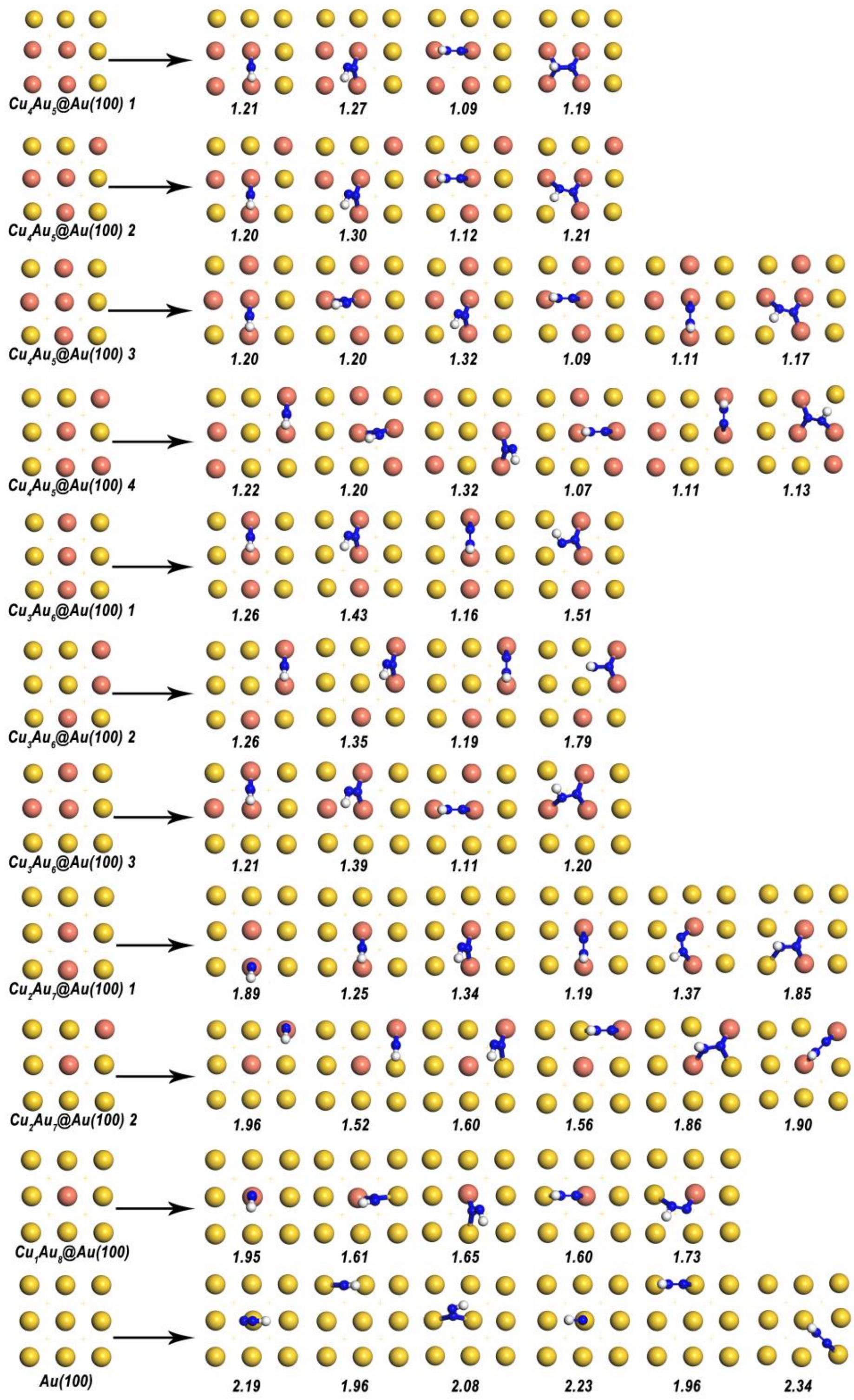

Figure S14. *NNH adsorption configurations considered for $Cu_nAu_{(9-n)}$@Au(100) with n = 0 to 4.

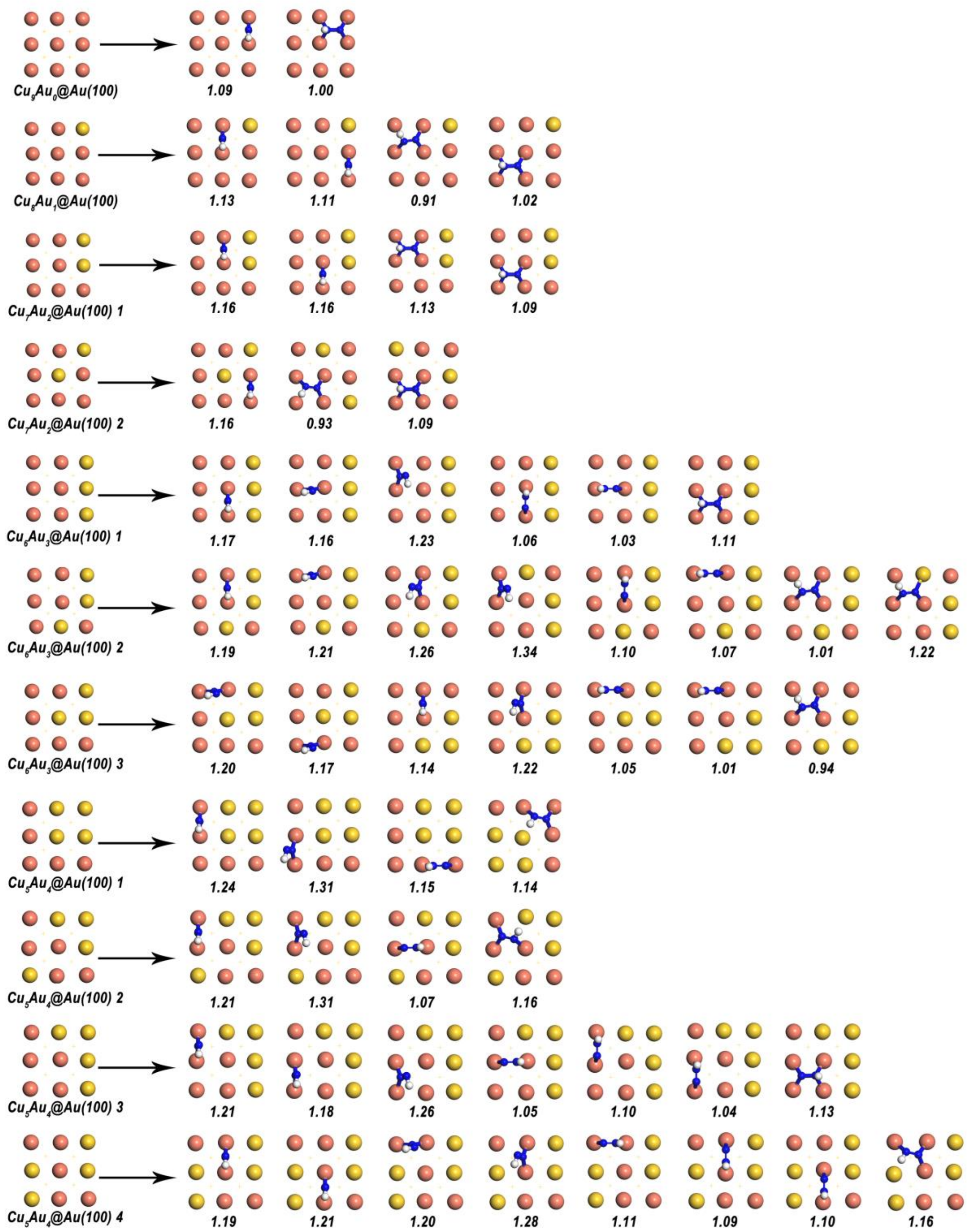

Figure S15. *NNH adsorption configurations considered for $Cu_nAu_{(9-n)}$@Au(100) with n = 5 to 9.

Figure S16. *NNH adsorption configurations considered for $Au_nCu_{(9-n)}$@Cu(100) with *n* = 0 to 4.

Figure S17. *NNH adsorption configurations considered for $Au_nCu_{(9-n)}$@Cu(100) with n = 5 to 9.

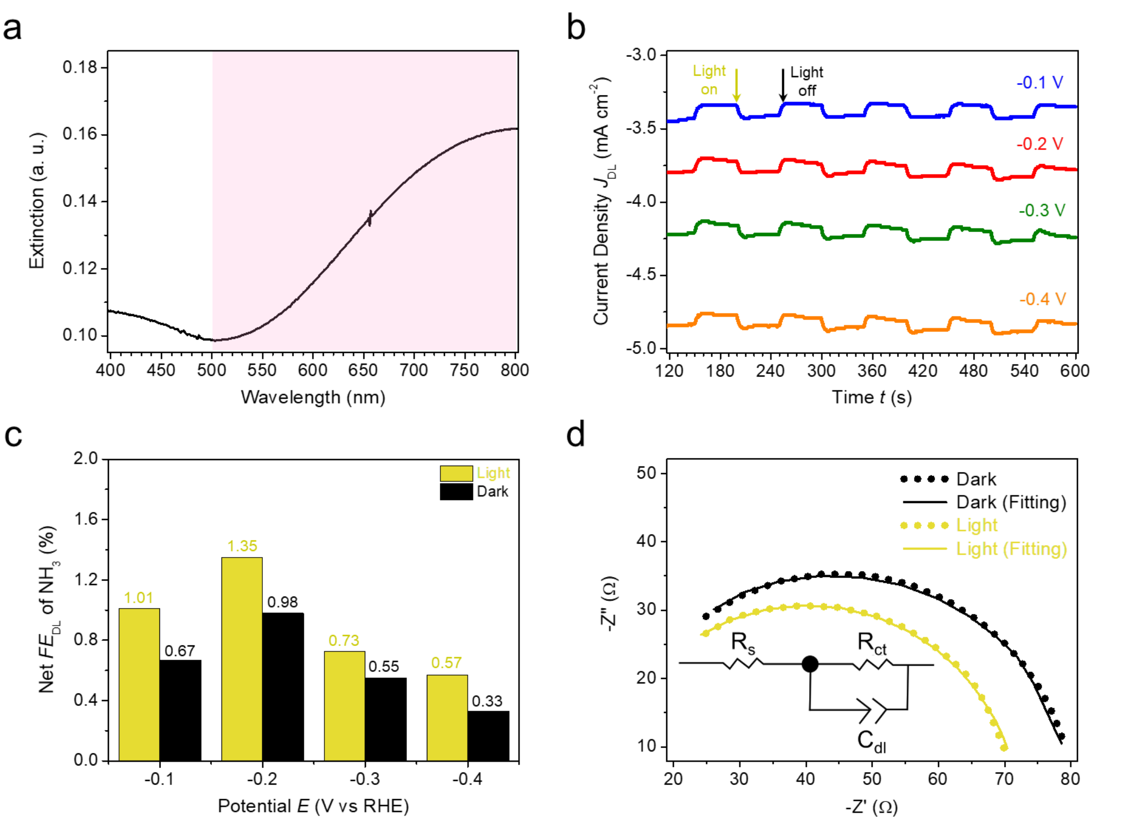

Figure S18. (a) UV-Vis spectra of suspended CuAu HNBs. (b) *J*-*t* plot of NRR catalyzed by CuAu HNBs under solar light (1 sun) with on-off switching. (c) Net NH_3 Faradaic efficiencies in N_2RR catalyzed by CuAu HNBs in dark and under solar light illumination. (d) Nyquist plots for CuAu HNBs in dark and under solar light illumination.

Table S1. Summary of N_2 reduction to NH_3 in aqueous solution at ambient conditions

Cathode Materials	**Electrolyte**	**FE of NH_3 at *E* (vs RHE)**	**References**
Li^+-incorporated PEBCD	0.5 M Li_2SO_4	1.71% at –0.7 V	*J. Am. Chem. Soc*. **2017**, *139*, 9771−9774
$Pd_{0.2}Cu_{0.8}$/RGO	0.1 M KOH	0.6% at –0.2 V	*J. Mater. Chem. A* **2018**, *6*, 17303−17306
spinel Fe_3O_4 nanorods on Ti mesh	0.1 M Na_2SO_4	2.6% at –0.4 V	*Nanoscale* **2018**, *10*, 14386−14389.
TiO_2/Ti	0.1 M Na_2SO_4	2.50% at –0.7 V	*ACS Appl. Mater. Interfaces* **2018**, *10*, 28251–28255
NiO nanodots on graphene	0.1 M Na_2SO_4	7.8% at –0.7 V	*ACS Appl. Energy Mater*. **2019**, *2*, 2288–2295
Cr_2O_3-rGO	0.1 M HCl	7.33% at –0.6 V	*Inorg. Chem*. **2019**, 58, 2257–2260
$Cr_{0.1}CeO_2$ nanorods	0.1 M Na_2SO_4	3.84% at –0.7 V	*Inorg. Chem*. **2019**, 58, 5423–5427
Ultrathin $Ni_{0.50}Fe_{0.50}$B nanosheets	0.1 M KOH	3.19 % at –0.3 V	*ACS Appl. Energy Mater*. **2020**, 3, 9516–9522
CoS_2 nanoparticles-embedded N-doped carbon nanobox derived from ZIF-67	0.1 M HCl	4.6% at –0.15 V	*ACS Sustainable Chem. Eng*. **2020**, 8, 29–33
CuAu nanocage on carbon paper	0.1 M KOH, N_2	7.4% at –0.2 V	This work